

Mapping brain function using a 30-day interval between baseline and activation: a novel arterial spin labeling fMRI approach

Ajna Borogovac¹, Christian Habeck², Scott A Small^{2,3} and Iris Asllani⁴

¹Department of Biomedical Engineering, Columbia University, New York, New York, USA; ²The Taub Institute for Research on Alzheimer's Disease and the Aging Brain, New York, New York, USA; ³Department of Neurology, Columbia University, New York, New York, USA; ⁴Department of Radiology, Columbia University, New York, New York, USA

By comparing hemodynamic signals acquired immediately before and during activation, functional magnetic resonance imaging (fMRI) is well suited for mapping acute changes in brain function. However, it remains unclear whether fMRI can map functional changes over longer periods. Here, we address this issue by empirically testing the feasibility of arterial spin labeling (ASL) fMRI to detect changes in cerebral blood flow (CBF) with baseline and task separated by 1 month. To increase the sensitivity of the method, we applied an algorithm that yielded flow density (CBFd) images that were independent of tissue content. To increase the accuracy, we developed a technique that generated arterial transit time at each voxel, independently. Results showed that activation changes in CBFd during the same session were statistically the same as across 30 days. The activation CBFd on day-30 was 34% (motor) and 25% (visual) higher than the respective baselines of 83 and 107 mL/100 g/min obtained on day-1. Furthermore, the signal-to-noise ratio of the CBFd measurement was 2.1 and 2.9 times higher than that of the conventional CBF for within-subject and across-subjects comparisons, respectively ($n=9$ healthy young subjects). Taken together, these results indicate that CBFd measure could be better suited than net CBF to map long-term changes in brain function.

Journal of Cerebral Blood Flow & Metabolism (2010) **30**, 1721–1733; doi:10.1038/jcbfm.2010.89; published online 21 July 2010

Keywords: ASL; arterial transit time; baseline drift; CBF; fMRI; 1/f noise; PVE

Introduction

Functional magnetic resonance imaging (fMRI) has emerged as an important tool for mapping the brain's response to external stimuli, disease, and various behavioral and pharmacological interventions. Currently, the prevailing technique is blood oxygenation level-dependent (BOLD) fMRI, whose contrast relies on local changes in magnetic field that are induced by the brain's hemodynamic response to a local change in neuronal activity (Ogawa *et al*, 1993). Consequently, the BOLD signal reflects a complex interaction of several physiological parameters and is generally expressed as a unitless relative measure.

Because of baseline drift effects, BOLD fMRI is unsuitable for detecting slow-varying changes in brain function (Aguirre *et al*, 2002; Wang *et al*, 2003; Zarahn *et al*, 1997) such as those due to chronic and gradually progressive disorders, and for mapping interventions the purported effect of which emerges over a longtime (e.g., physical exercise, Pereira *et al*, 2007). The power spectrum of the BOLD signal shows higher amplitudes at low frequencies due to what has been described as the 1/f noise (Zarahn *et al*, 1997). This temporal autocorrelation makes BOLD fMRI unfeasible for experimental designs with fundamental frequency below 0.01 Hz; that is, for task events more than ~90 seconds apart (Zarahn *et al*, 1997).

More recently, perfusion-based techniques such as arterial spin labeling (ASL) fMRI have been developed to map brain function during rest and activation. ASL measures cerebral blood flow (CBF) directly by working on an entirely different principle from BOLD. In ASL, the proton spins of the arterial blood water are 'labeled' before they perfuse into the

Correspondence: Dr I Asllani, Department of Radiology, Columbia University, New York, NY, USA.

E-mail: ia2026@columbia.edu

This study was funded in part by the NIH grant: NIA 5R01AG026114-02.

Received 13 February 2010; revised 19 May 2010; accepted 23 May 2010; published online 21 July 2010

tissue (Williams *et al*, 1992). Depending on the method used for labeling, ASL techniques are commonly classified as continuous ASL (CASL), pulsed ASL, or velocity-selective ASL. Herein, we present results from CASL. However, the methodology and conclusions should be applicable to other ASL techniques.

In CASL, the 'labeled' image is acquired after the inversion of the arterial water spins by an adiabatic sequence consisting of a relatively long off-resonance radiofrequency pulse and a constant gradient in the direction of the flow (Williams *et al*, 1992). A 'control' image is also acquired after the same sequence but with a sine-modulated radiofrequency pulse to ideally produce no net magnetic inversion of the spins (Alsop and Detre, 1998). A CBF image is computed by subtracting the labeled from the control image and then applying a set of measured or assumed physiological and MRI parameters to obtain voxelwise flow values in absolute units (e.g., mL/100 g/min).

Because the ASL signal originates from the difference between two images, it is spared the baseline drift effects present in BOLD—that is, the noise power spectra of the ASL signal is approximately flat across the entire sampling frequency range. Consequently, in contrast to BOLD, ASL can, at least theoretically, be used to map slow-varying changes in brain function without a time restriction in the spacing of the events.

Another advantage of ASL versus BOLD is that the ASL signal is expressed in physiologically meaningful units and provides a direct measure of a physiological correlate of brain activation, namely, CBF. Thus, ASL fMRI allows for direct comparison of both baseline and activation CBF across subjects, scan sessions, and other imaging modalities that measure CBF such as ^{15}O PET (Golay *et al*, 2004).

The primary aim of this study was to empirically investigate the feasibility of ASL fMRI for detecting absolute changes in CBF due to motor–visual activation with baseline and task images acquired 1-month apart (corresponding to a task frequency of $\sim 3.7 \times 10^{-7}$ Hz).

Toward this goal, we began by improving the sensitivity and accuracy of the ASL measurement. First, we applied a recently developed algorithm that corrects for partial volume effects (PVEc) in ASL imaging (Asllani *et al*, 2008a). An advantage of PVEc ASL is its ability to yield tissue-specific 'flow density' (CBFd) images that are independent of voxels' tissue content (Asllani *et al*, 2008a). That is, for each voxel and a given tissue, CBFd is the amount of flow the voxel would have if it were comprised entirely of that tissue (Asllani *et al*, 2008a). We hypothesized that because CBFd is less affected by spatial and inter-subject variability in tissue content, it would be more sensitive for detecting changes in CBF than the conventional ASL method (Asllani *et al*, 2009b).

Second, to increase the accuracy of the quantification of CBF, we combined the PVEc method with a multiple labeling duration acquisition to obtain whole-brain voxelwise arterial transit time (ATT)

images in standard space. At each voxel, ATT represents the time it takes the labeled water to cross the arterial distance from the labeling plane (commonly positioned in the carotids) to the vasculature system within that voxel (Alsop and Detre, 1996). Arterial transit time can be estimated via a parametric fit of the curves representing the fractional ASL signal versus time (Alsop and Detre, 1996; Asllani *et al*, 2008b; Parkes and Tofts, 2002; Wong *et al*, 1997; Ye *et al*, 1997). However, because this step requires relatively long scanning times, ATT is not routinely measured in ASL imaging. Instead, when computing the CBF, ATT values are generally assumed to be either homogeneous throughout the brain or uniformly distributed within an acquisition slice and varying linearly with the ascending slice positions (Asllani *et al*, 2008a; Asllani *et al*, 2008b; Hermes *et al*, 2007; Parkes *et al*, 2004; Rashid *et al*, 2004). In a study by Wong *et al* (1997), voxelwise fitting of ATT data was obtained but restricted only to voxels with high gray matter (GM) content, which, however, was not specified. More recently, Hendrikse *et al* (2008) obtained voxelwise maps of ATT that revealed regional heterogeneity of blood arrival times even within a slice. However, the ATT maps represented only partial coverage of the brain and no correction was performed for the mixing of the signals because of PVE. Here, by combining PVEc algorithm with a more efficient acquisition method, we estimated ATT for each tissue and at each voxel, independently.

The work presented herein shows the unique versatility of the ASL perfusion fMRI for detecting changes in CBF with very low task frequency, and offers important insights on the accuracy, reproducibility and sensitivity of the CBF and the ATT measurements with ASL.

Materials and methods

Subjects

ATT experiment: Arterial transit time images were obtained on seven healthy young subjects (age = 26 ± 6 years, 4 men) as described below. Five of these subjects (age = 23.6 ± 5 years, 2 men) were also part of the functional activation study.

Activation experiment: Arterial spin labeling CBF images were obtained from a group of healthy young subjects ($n = 9$, age = 24 ± 4 years, 4 men) on two separate imaging sessions, 1-month apart, referred to as D1 and D30. In four of the subjects, the activation paradigm was repeated twice, for two different values of the postlabeling delay (PLD), as described below.

There was no significant age difference between the subjects who participated in the ATT experiment and the activation experiment ($P = 0.42$, $\alpha = 0.05$).

All subjects were instructed to keep similar daily and sleeping routines throughout the study and were asked to avoid food for 2 hours, caffeine for 8 hours, and alcohol for

48 hours before each scanning session. Written informed consent was obtained from all participants according to Columbia University's Institutional Review Board guidelines.

Image Acquisition

All imaging was performed on a 3T scanner (Philips Achieva, Best, Netherlands) using a transmit–receive head coil provided by the manufacturer. To obtain tissue content information, a high-resolution magnetization prepared rapid gradient echo (MPRAGE) was acquired on each subject with the following parameters: repetition time/echo time = 6.7/3.1 ms, inversion time = 0.8 s, flip angle = 8°, spatial resolution = 0.9 × 0.9 × 0.9 mm³, 180 image slices.

ATT measurement: For each subject, CASL baseline images were acquired at 13 different labeling durations (LD), ranging 100 to 1000 ms, step of 100 ms, and 1000 to 1600 ms, step of 200 ms.

For each LD value, 15 ASL control/label pairs were acquired with: field of view = 240 × 210 mm², in plane resolution = 3.75 × 3.75 mm², slice thickness/gap = 8.0 mm/1.2 mm, PLD for the 1st acquired slice, henceforth referred to as PLD_{min}, was 50 ms, number of slices = 15, slice acquisition time = 72 ms.

To avoid saturation effects, slices were acquired in an interleaved (step of 2) descending order (superior to inferior) in three separate slice-packages; the repetition time/echo time per package was 3600/29 ms.

Activation experiment: Both D1 and D30 sessions consisted of 5 OFF-ON blocks, 2 minutes each (that is, 13 ASL CBF images per condition). OFF denotes the baseline acquisition, during which the subject fixated on a small white cross presented at the center of the subject's field of view, whereas ON represents activation, during which subjects performed simultaneous motor and visual tasks. The visual stimulus consisted of an 8 Hz reversing black/white checkerboard generated with E-prime (Psychology Software Tools, Sharpsburg, PA, USA) and was presented using MRI-compatible video goggles (VisuaStim Digital, Resonance Technology, Los Angeles, CA, USA). The motor task consisted of self-paced right-hand sequential button pressing (Current Designs fORP button box, Philadelphia, PA, USA). The visual stimulus provided the cue for the motor task.

The CASL CBF acquisition was similar to that of ATT measurement with the exception of the following parameters: repetition time = 4300 ms, LD = 1920 ms, PLD_{min} = 500 ms, 13 slices in ascending acquisition order, 1 package. To check for the effect of PLD on CBF quantification, the activation experiment was repeated on four subjects using PLD_{min} = 1000 ms.

Image Processing

CASL EPI images were motion corrected separately for each imaging session (D1, D30, and ATT measurement) using statistical parametric mapping (SPM5) (Friston *et al*, 1996). Each subject's MPRAGE was segmented (Ashburner and Friston, 2005) to obtain voxelwise GM,

white matter (WM), and cerebrospinal fluid (CSF) content images as posterior probability maps, P_{GM}, P_{WM}, and P_{CSF} respectively (Asllani *et al*, 2008a).

Voxelwise ATT measurement: The following processing steps were performed to obtain the ATT images: (1) For each LD value, GM ASL fractional signal images (computed as percent change between control and label images), were obtained using the PVEc algorithm as detailed in Asllani *et al* (2008a). A regression kernel size = 5 × 5 × 1 voxels was applied. It is important to emphasize that for each voxel, the GM fractional signal represents the ASL signal per unit GM volume and is, therefore, theoretically independent of the voxel's GM content (Asllani *et al*, 2008a; Asllani *et al*, 2009b).

(2) A voxelwise parametric fitting of the fractional signal versus LD was performed using the Levenberg–Marquardt least squares algorithm. The CBF_d values were constrained to vary within the (107 ± 40) mL/100 g/min range, representing mean ± 2 s.d. of the estimated CBF_d for this population (Asllani *et al*, 2009b). The remaining parameters, such as arterial and tissue T1, were set to the values listed in the 'CBF computation' section below. The one-compartment theoretical model was assumed for the fit (Golay *et al*, 2004).

(3) For each subject, the voxelwise ATT values obtained from the parametric fit in step (2) were used to construct the ATT image that was then normalized to the MNI space for subsequent group analysis. The normalization was performed using the SPM5 unified segmentation and normalization algorithm (Ashburner and Friston, 2005).

Activation experiment: ASL images were analyzed using a slightly modified version of the PVEc algorithm reported in Asllani *et al* (2008a). To avoid the oversmoothing of the data at the border of the activated and nonactivated regions, the shape of the linear regression kernel was modified as follows: if a given voxel was hypothesized as activated, then only the other hypothesized activated voxels in its neighborhood would contribute to its linear regression kernel. Conversely, if a given voxel was hypothesized as non-activated, its activated neighbors were excluded from its regression kernel (Asllani *et al*, 2009a). A voxel was hypothesized as activated if its ΔCBF_d = 15 mL/100 g/min, representing 1 s.d. from the average baseline CBF. It is crucial to emphasize that hypothesizing a voxel as 'activated' will not in itself cause it to appear activated post-analysis; these steps only modify the regression kernel to minimize its smoothing effect (Asllani *et al*, 2009a).

CBF computation: GM and WM CBF_d images were obtained as detailed in the study by Asllani *et al* (2008a). Postlabeling delay was adjusted to account for the inter-slice acquisition time, PLD = ((acquisition slice # - 1) × 72 + PLD_{min}) ms. To check for the effect of PLD on CBF quantification, CBF images were also acquired with PLD_{min} = 1000 ms as described above.

Gray matter ATT at each voxel was assigned based on the group average GM ATT computed across the seven subjects

who participated in the multi-LD experiment. Tissue transit time (TTT) was modeled to vary linearly with ATT with an additional exchange time assumed to be 500 and 700 ms for GM and WM, respectively (Asllani *et al*, 2008a).

Other parameters used for CBF quantification were: arterial spin-lattice and spin-spin relaxation times, $T1a = 1740$ ms (Greenman *et al*, 2003; Stanisiz *et al*, 2005) and $T2a = 275$ ms (Stanisiz *et al*, 2005), respectively; blood/tissue water partition coefficient, $\lambda = 0.98$ and 0.82 mL/g for GM and WM, respectively (Herscovitch and Raichle, 1985); tissue $T1$ in the absence of RF, $T1ns = 1540$ and 1009 ms for GM and WM, respectively (Bandettini, 2001; Ethofer *et al*, 2003; Stanisiz *et al*, 2005; Wansapura *et al*, 1999); $T1$ in the presence of RF, $T1s = 1078$ and 706 ms for GM and WM, respectively (Wang *et al*, 2002); tissue $T2 = 110$ and 80 ms for GM and WM, respectively (Bandettini, 2001; Gelman *et al*, 1999; Stanisiz *et al*, 2005). Labeling efficiency for 3T was assumed $= 0.7$ (Wang *et al*, 2005).

At each voxel, PVE-corrected net CBF images were computed as: $CBF_{net} = (P_{GM} \cdot CBFd_{GM}) + (P_{WM} \cdot CBFd_{WM})$, where P_{GM} and P_{WM} represent the fractional tissue content of GM and WM in a given voxel, respectively (Asllani *et al*, 2008a).

To compare signal-to-noise ratios (SNR) across methods, ASL CBF images were also computed using the conventional, PVE-uncorrected, method (Asllani *et al*, 2008a).

Data Analysis

Computation of SNR for the voxelwise ATT measurement: To evaluate inter-subject variability in regional ATT, average (μ) and s.d. (σ) GM ATT were computed at each voxel across the seven participants of the multi-LD experiment. This process yielded a μ and a σ image for the entire group.

The primary motor and visual cortices were identified using Picketlas (Maldjian *et al*, 2003; Maldjian *et al*, 2004), and were based on a composite of Brodmann areas 1, 2, 3, 4 for the motor regions of interest (ROI), and 17, 18, 19 for the visual ROI. To include any anatomical variability across subjects in these ROIs, they were dilated by five voxels (motor) and three voxels (visual).

Assessment of the effect of ATT on CBF quantification: The ATT measurement of this study incorporated two novel aspects: (1) It used the PVEc algorithm for separating the WM ATT from the GM ATT. (2) It fitted the data for each voxel independently, thus making no assumptions about the voxel's position.

To show the advantage of this method, GM CBFd images yielded based on it were compared with those acquired based on: (1) ATT maps obtained from fitting of the conventional, PVE-uncorrected data, and (2) slice-wise fitting of the average fractional signal from voxels with high GM tissue content ($P_{GM} > 0.7$) (Asllani *et al*, 2008b; Hirohiko *et al*, 2004; Parkes and Tofts, 2002). This step assumes ATT to be homogeneously distributed within a slice with an initial value given to the first slice, which is then linearly incremented with superior slices. Here, this step was modeled as: $ATT_n = ATT_1 + 112(n-1)$ ms, where:

n = slice number, $ATT_1 = ATT$ of the first slice = 200 ms (Parkes and Tofts, 2002), and 112 ms = the ATT increment per slice computed as the average of findings of Parkes and Tofts (2002) and Asllani *et al* (2008b).

Functional activation experiment: Data were analyzed using both voxelwise and ROI wise approaches.

Voxelwise analysis: First level, subject-wise SPM analysis was performed using GM CBFd images for four different contrasts: $(D1_{ON} - D1_{OFF})$, $(D30_{ON} - D30_{OFF})$, $(D1_{ON} - D30_{OFF})$, $(D30_{ON} - D1_{OFF})$. It is to noted that the first and the second contrasts compare activation and baseline images acquired within the same scanning session, which we refer to as 'within session' comparison, whereas the third and fourth contrasts compare activation and baseline images acquired 1-month apart, and is thus referred to as over-1-month comparison.

As a check for the test-retest reliability of the ASL signal, baseline contrasts $(D1_{OFF} - D30_{OFF})$ and $(D30_{OFF} - D1_{OFF})$ were also compared.

ROI analysis: At the subject level, the activation ROIs were defined as the collection of voxels that survived the statistical threshold ($T = 2.6$, $P_{uncorrected} < 0.005$) for subject's first level analysis. Group activation ROIs were obtained by conjoining all the voxels that survived the statistical threshold from each subject. A paired t -test ($\alpha_{uncorrected} = 0.05$) analysis was run to determine if the difference in D1 and D30 baseline CBFd and the difference in D1 and D30 $\Delta CBFd$ were statistically significant.

Comparison of PVEc with the conventional ASL method: To show the advantage of the PVEc method over the conventional ASL, we compared the SNR of three measurements: net CBF obtained with the conventional, PVE-uncorrected, method; net CBF obtained using PVEc; and GM CBFd, which is a novel parameter yielded by the PVEc method. Signal-to-noise ratio was defined as the inverse of coefficient of variation, which is denoted as $(\sigma/\mu)_{inter-subject}$ and $(\sigma/\mu)_{intra-subject}$ for across-subjects and within-subject computations, respectively.

Effect of PLD on activation measurement: To investigate the effect of the relatively short $PLD_{min} = 500$ ms on the quantification of both baseline and activation GM CBFd, on four subjects, the activation paradigm was repeated for $PLD_{min} = 1000$ ms. In all cases, the $PLD_{min} = 1000$ ms acquisition followed the $PLD_{min} = 500$ ms. A paired t -test was used to compare the D30 baseline CBFd measured using $PLD_{min} = 500$ ms and $PLD_{min} = 1000$ ms acquisitions.

Results

Quantification of CBF and Regional Heterogeneity of ATT

Blood arrival times were shortest (200 to 300 ms) in the circle of Willis and the deep middle cerebral artery (MCA) and anterior cerebral artery (ACA) territories (Figure 1, second row). Subject-wise

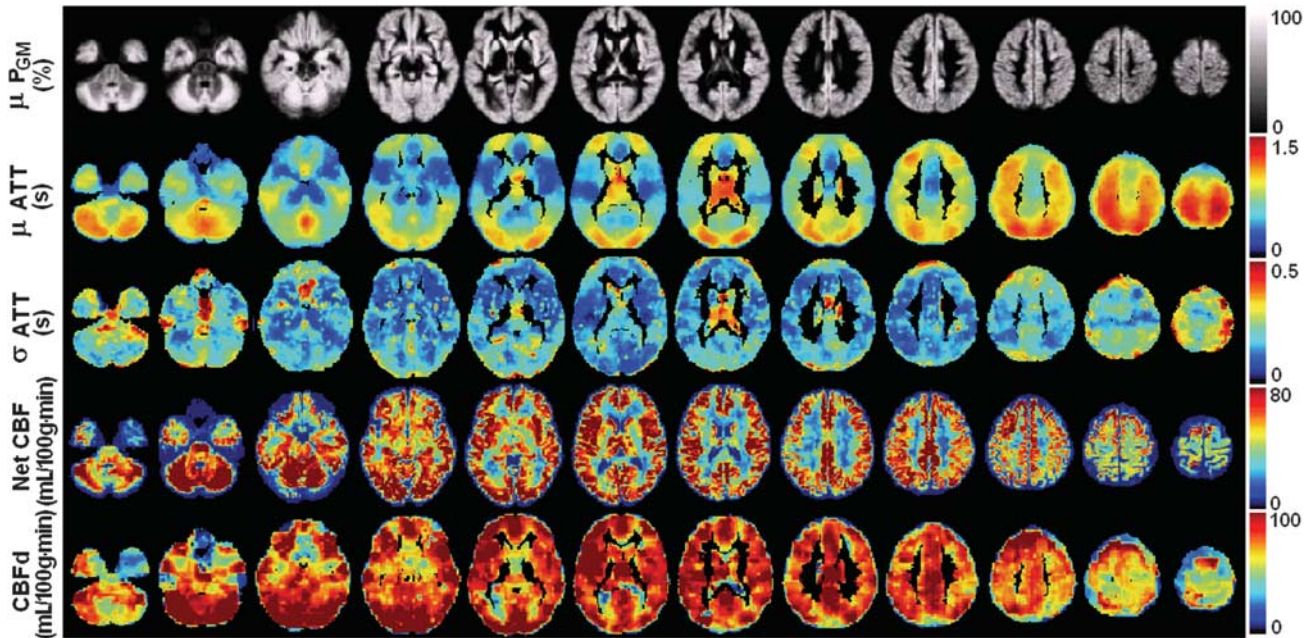


Figure 1 Arterial transit time (ATT) measurement and cerebral blood flow (CBF) quantification. Subject-wise mean (μ) GM ATT (second row) and s.d. (σ) of ATT (third row). For anatomical reference, the group-averaged GM posterior probability maps are shown in the first row. Fourth and fifth rows show net CBF and CBFd images from a randomly selected subject. Slices correspond to the MNI z-coordinates (−42 to 68) mm, with a 10 mm increment. Only voxels with $P_{GM} > 1.5\%$ are shown.

average ATT in the motor and visual ROIs were 1037 ± 108 and 875 ± 88 ms, respectively. Importantly, there was substantial within-slice heterogeneity (Figure 1, second row) with longer ATT values (800 to 1500 ms) found in the cerebellum, occipital lobe, and watershed regions. The inter-subject s.d. throughout most of the brain was < 200 ms with focal specks of higher s.d. found mostly in the brain edges and regions with high CSF content (Figure 1, third row).

To give a qualitative sense of flow images, net CBF and GM CBFd images from a randomly selected subject are shown in Figure 1, fourth and fifth rows, respectively. Note that while the net CBF images contain tissue contrast, the signal intensity of the CBFd images is uniformly distributed as it mainly reflects the tissue-independent flow density values.

Owing to scanning time restrictions, ATT images are not routinely acquired in ASL studies. Instead, ATT is modeled based on two main assumptions: (1) within-slice homogeneity, and (2) linear increase with superior slices (Asllani *et al*, 2008a; Asllani *et al*, 2008b; Kimura *et al*, 2004; Parkes *et al*, 2004). The effects of these assumptions on quantification of CBF are shown in Figure 2A, in which CBFd images obtained based on modeled ATT were compared with those experimentally acquired at each voxel, independently. On average, the largest effect was observed in the occipital lobe, thalamus, cerebellum, and the deep ACA and MCA territories (Figure 2A).

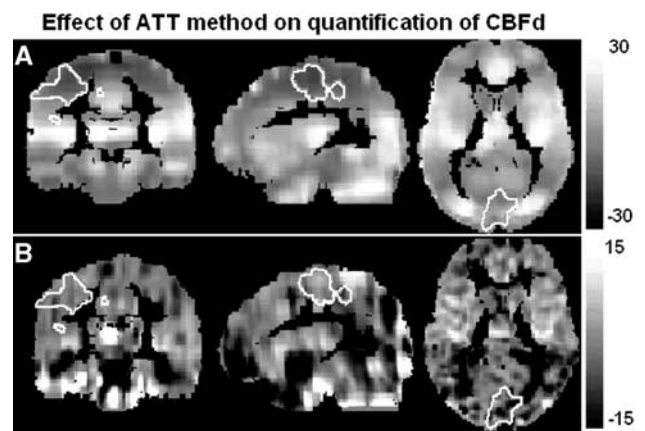


Figure 2 Advantage of the new method for estimation of arterial transit time (ATT). (A) The difference images between the GM CBFd obtained experimentally from the partial volume effect-corrected (PVEc) method developed here (by voxelwise fitting of the multiple labeling duration (LD) data) and the GM CBFd based on the modeled ATT (by linearly incrementing it with each slice and assuming it to be homogenous within the slice). Note the effects in occipital lobe, cerebellum, thalamus, and the vascular territories. (B) The difference images of GM CBFd computed with ATT based on the PVEc method and ATT based on conventional ASL method. Note that the largest effect is in the areas with high tissue heterogeneity. The motor and visual ROIs are delineated with a white line. The shown slices were located at MNI coordinate = (22, −44, 6 mm). Only voxels with GM content $> 1.5\%$ are shown.

The advantage of the PVEc method versus the conventional ASL method is shown in Figure 2B. As expected, the largest discrepancy was

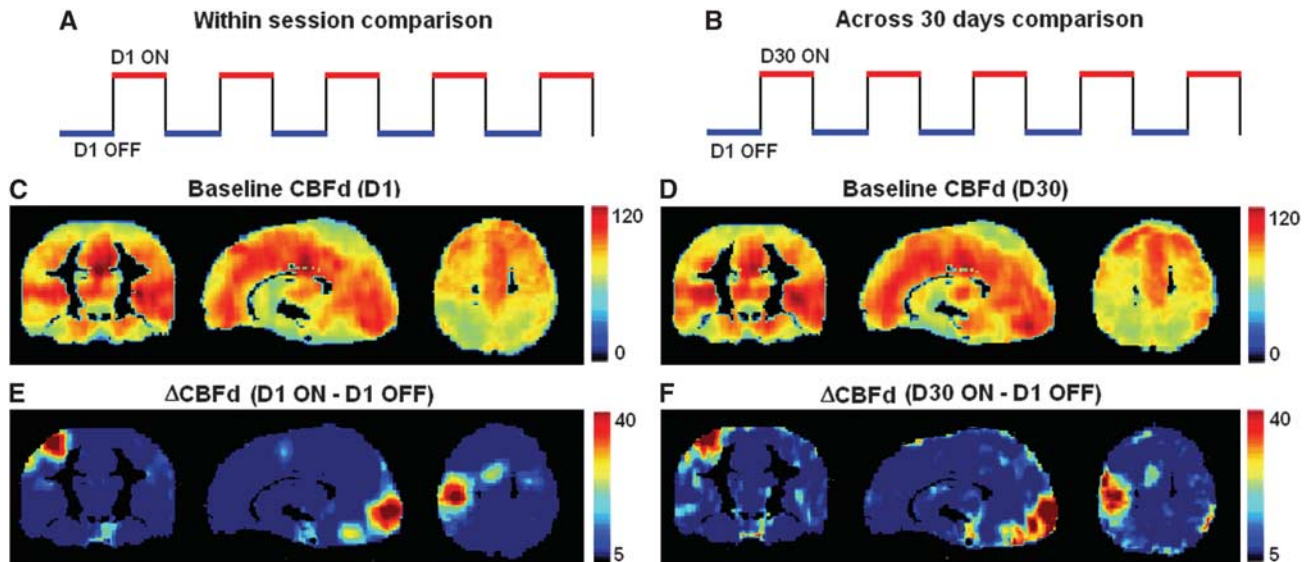


Figure 3 Comparison of baseline CBFd and activation Δ CBFd across sessions. Panels **A** and **B** show the diagrams of the comparisons used for within-session and over-1-month contrasts, respectively. To get a sense of the images used, subject-wise average baseline gray matter (GM) CBFd (mL/100g/min) are shown in panels **C** and **D** for D1 and D30 acquisitions, respectively. Panel **E** shows the within-session difference in GM CBF, Δ CBFd (computed as $(D1_{ON} - D1_{OFF})$), whereas panel **F** shows over-1-month Δ CBFd (computed as $(D30_{ON} - D1_{OFF})$) for D30. Note the increase in GM Δ CBFd in primary visual and motor cortices, supplementary motor area (SMA) and the cerebellum, with the remaining brain regions being relatively spared. Slices shown were chosen to depict both motor and visual activation and were located at the MNI coordinates = (10, -20, 56 mm).

found in the areas with high tissue heterogeneity (Figure 2B).

ASL fMRI can Detect Changes in CBF when Baseline and Activation are Separated by 1 Month ($f_{\text{task}} \approx 3.7 \times 10^{-7}$ Hz)

Voxelwise analysis: As a measure of test-retest reliability of the ASL CBF measurement, the group-averaged baseline CBFd images obtained on D1 (Figure 3C) were compared with those from D30 (Figure 3D). No voxels survived the statistical threshold ($t_{\text{two-tailed}} = 4.5$, $P_{\text{uncorrected}} < 0.001$, extent threshold $k > 50$ voxels) for either $(D30_{OFF} - D1_{OFF})$ or $(D1_{OFF} - D30_{OFF})$ contrasts.

The activation Δ CBFd images, computed as: $(\text{CBFd}_{\text{activation}} - \text{CBFd}_{\text{baseline}})$, are shown in Figures 3E and 3F for the within-session ($D1_{ON} - D1_{OFF}$) and over-1-month ($D30_{ON} - D1_{OFF}$) comparisons, respectively; the corresponding T-maps overlaid on a glass brain are shown in Figure 4.

In the motor cortex, the average Δ CBFd was 22 and 30 mL/100 g/min for the within-session and over-1-month comparisons, respectively. In the visual cortex, the mean Δ CBFd was 25 mL/100 g/min for the within-session and 34 mL/100 g/min, for the over-1-month contrasts. In both motor and visual ROIs, the number of voxels that survived the statistical threshold ($T = 3.0$, $P_{\text{uncorrected}} < 0.001$) was $\sim 50\%$ higher for the within-session contrast.

To give a qualitative sense of the subject-wise activation patterns, Δ CBFd images for both within-

session and over-1-month comparisons are shown in Figure 5 for each subject. Visual inspection indicates that both the magnitude and the spatial extent of Δ CBFd vary across subjects and task frequency. In the following section, we quantify these results at the ROI level.

Regions of interest analysis: For each subject, baseline and activation CBFd values are shown in Figures 6A and 6B for the motor and visual cortex ROIs, respectively. At the group level, there was no effect of day on the reproducibility of the baseline GM CBFd for either ROI ($P > 0.9$, $\alpha = 0.05$, for both ROIs). The group-average activation Δ CBFd in the motor cortex was 30 ± 6 and 28 ± 7 mL/100 g/min for D1 and the D30, respectively, corresponding to a 35% increase in CBFd relative to the baseline. In the visual cortex ROI, these values were 30 ± 7 and 27 ± 6 mL/100 g/min for D1 and D30, respectively, corresponding to 26% increase in GM CBF. There was no effect of day on Δ CBFd values in either ROI ($P > 0.4$, $\alpha = 0.05$, for both ROIs).

Partial Volume Effect-Corrected ASL has Higher Sensitivity in Detecting Activation Changes in CBF than the Conventional ASL Method

The net CBF inter-subject coefficient of variation, $(\sigma/\mu)_{\text{inter-subject}}$, images obtained using the conventional, PVE-uncorrected method are compared with those yielded by PVEc in Figure 7A, first and second rows, respectively; the $(\sigma/\mu)_{\text{inter-subject}}$ image for the

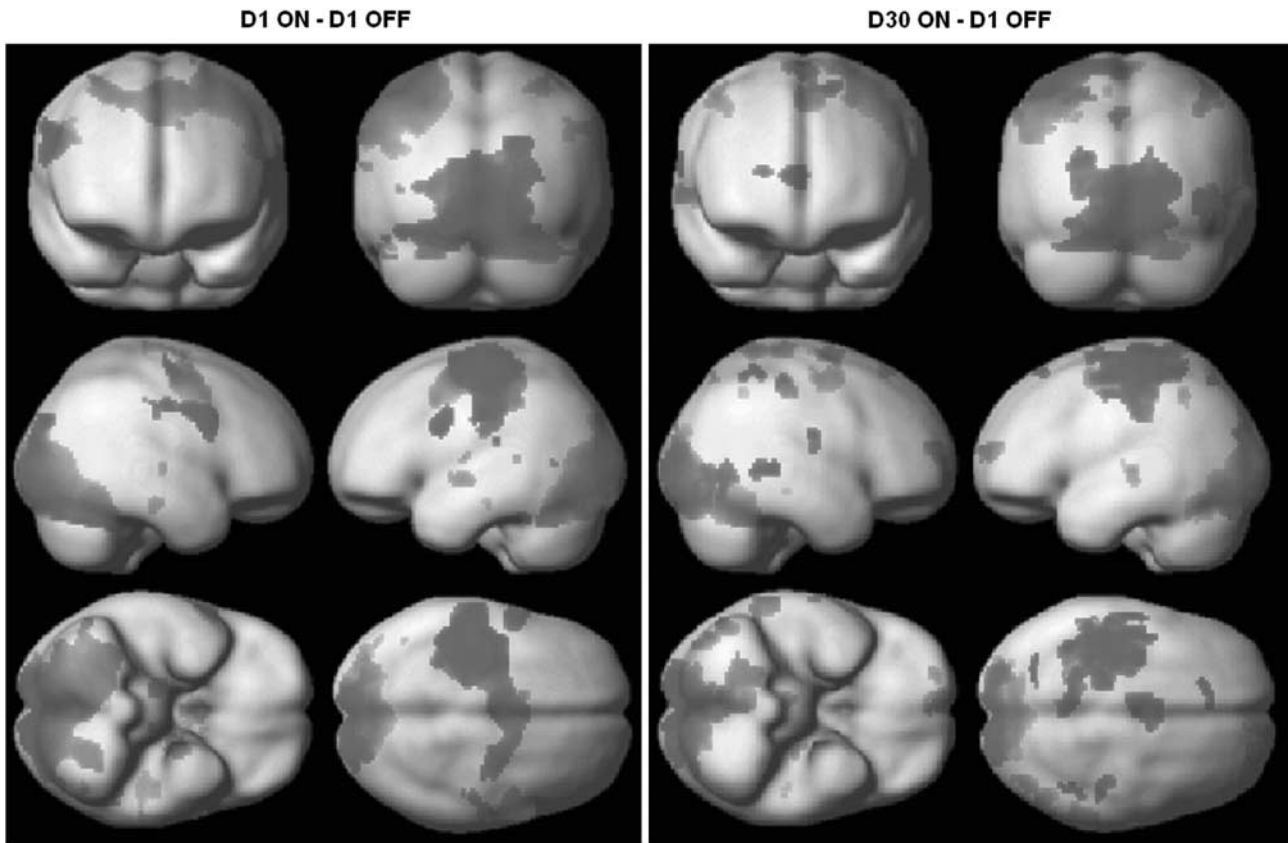


Figure 4 Group statistical parametric mapping (SPM) maps ($P_{\text{uncorrected}} > 0.005$), for the within-session contrast (A) and over-1-month (B). Note the similarity of the activation patterns between the two contrasts.

CBFd measurement is shown in the third row. Overall, $(\sigma/\mu)_{\text{inter-subject}}$ for the CBFd measurement was $\sim 30\%$ and $\sim 45\%$ lower than that of net CBF measured with PVEc and conventional ASL methods, respectively. There was no effect of ROI location on σ/μ for either method—the PVEc method yielded $(\sigma/\mu)_{\text{inter-subject}} = 0.27$ and 0.25 in the motor and visual ROIs, respectively, whereas for the conventional method these values were 0.57 and 0.51 .

The intra-subject coefficient of variability $(\sigma/\mu)_{\text{intra-subject}}$ in the motor cortex was 0.47 ± 0.15 versus 1.36 ± 0.74 for the CBFd and net CBF measurements, respectively; for the visual cortex, these values were 0.37 ± 0.10 and 1.06 ± 0.84 . Overall, $(\sigma/\mu)_{\text{intra-subject}}$ was $\sim 65\%$ lower for the PVEc CBFd measurement as compared with the conventional net CBF. In contrast to the inter-subject coefficient of variation, the intra-subject was dependent on the location of the ROI and was higher in the motor cortex for both PVEc and the conventional method. The difference, however, was only statistically significant when PVEc CBFd images were used ($P = 0.0004$), whereas for the conventional net CBF images the difference did not reach significance ($P = 0.17$).

The effect of SNR differences on detecting activation is shown in Figure 7B, where activation-baseline SPM(T)-maps obtained using conventional net CBF, PVEc net CBF, and PVEc CBFd images are shown.

The number of voxels that survived the statistical threshold ($T = 3.6$, $P_{\text{uncorrected}} < 0.001$) was $\sim 60\%$ higher for the PVEc CBFd measurement compared with the net CBF yielded by the conventional ASL method (4630 versus 2004 voxels and 7686 versus 3863 voxels in the motor and visual ROIs, respectively).

Effect of PLD on CBF Quantification

In the motor cortex, there was no effect of PLD on the baseline CBF—the subject-wise average baseline GM CBFd was 97 ± 11 mL/100 g/min and 94 ± 18 mL/100 g/min for PLD_{min} = 500 ms and PLD_{min} = 1000 ms acquisitions, respectively. In the visual cortex, however, the difference was substantial—the average baseline CBF for PLD_{min} = 1000 ms was ~ 24 mL/100 g/min lower than that for the PLD_{min} = 500 ms acquisition.

In both ROIs, the activation Δ CBFd was substantially lower, $\sim 38\%$, for PLD_{min} = 1000 ms acquisition as compared with the PLD_{min} = 500 ms. It is important to note that the ROI-based SNR (defined as the inverse of the coefficient of variation) of the PLD_{min} = 1000 ms was ~ 50 and 20% lower than that of PLD_{min} = 500 ms acquisition in visual and motor ROIs, respectively.

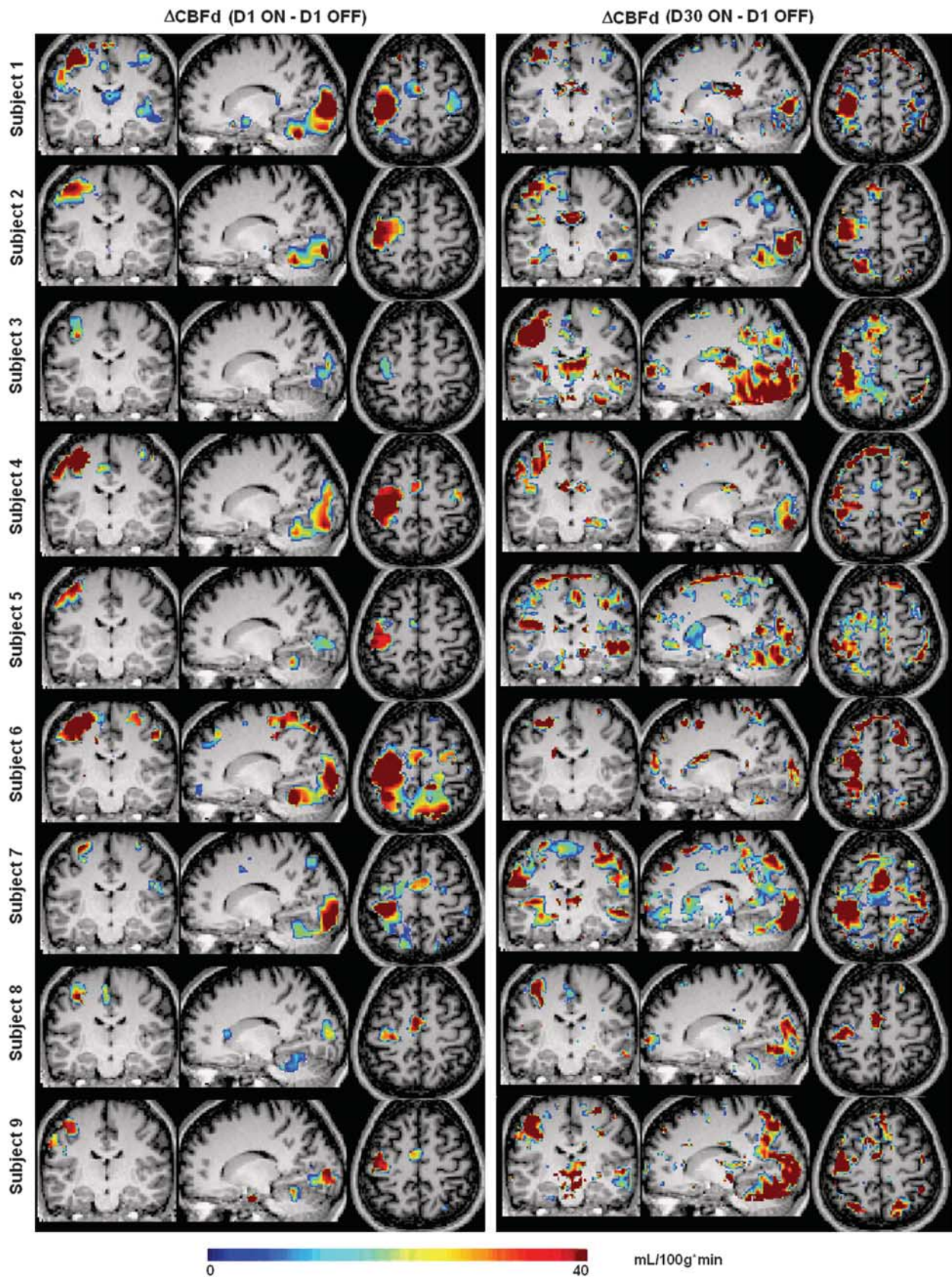


Figure 5 ΔCBFd images obtained from each subject for the within-session (first column) and over-1-month (second column). Colored regions include only voxels that survived the statistical threshold ($T = 2.6$, $P_{\text{uncorrected}} < 0.005$) of the first level analysis.

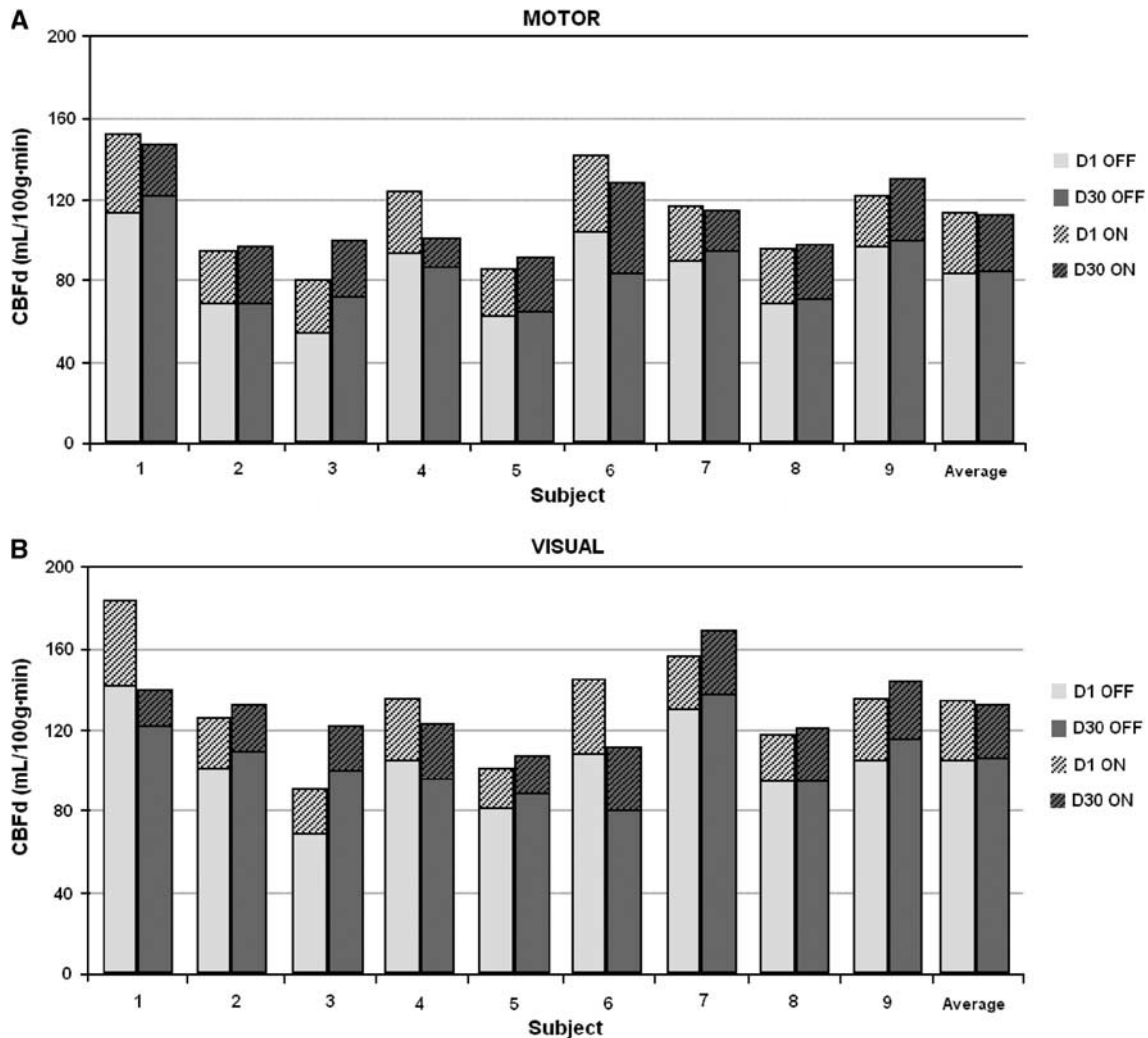


Figure 6 Regions of interest (ROI) analysis. For each subject, baseline (solid colors) and activation (stripes) gray matter (GM) CBFd for D1 (red) and D30 (blue) are shown for the motor ROI (A) and visual ROI (B). The rightmost columns on each panel show the corresponding subject-wise mean values.

Summary of Results

1. We found substantial variability in ATT values across the brain with the occipital lobe and the cerebellum having similar ATT with the superior regions. For the motor and visual ROIs, subject-wise average ATT was 1037 ± 108 and 875 ± 88 ms respectively.
2. There was no significant difference in baseline CBF across the two time points, D1 and D30, 30 days apart. Subject-wise average GM flow density was 83 ± 19 mL/100 g/min and 108 ± 21 mL/100 g/min in motor and visual regions, respectively, representing on average a 30% higher baseline GM flow density in the visual ROI versus the motor.
3. There was no significant difference in activation Δ CBFd across the two time points, 30 days apart, in either motor or visual ROI. Also, there was no statistical difference in Δ CBFd across activated regions; for both motor and visual ROIs group-

averaged Δ CBFd was $\sim 29 \pm 7$ mL/100 g/min, representing a 35% and 26% increase compared with their respective baseline values.

4. The PVEc method was found more sensitive in detecting changes in CBF than the conventional, PVE-uncorrected, method.

Discussion

This is the first study to empirically show the feasibility of ASL for detecting longitudinal changes in CBF due to functional activation with very low task frequency ($f_{\text{task}} \sim 3.7 \times 10^{-7}$ Hz), that is, with task and baseline acquired 1-month apart. The activation paradigm consisted of a motor-visual stimulation, which was chosen because it induces an increase in CBF in several distinct and well-established anatomical regions, thus ensuring that the detected change was indeed due to functional activation and not

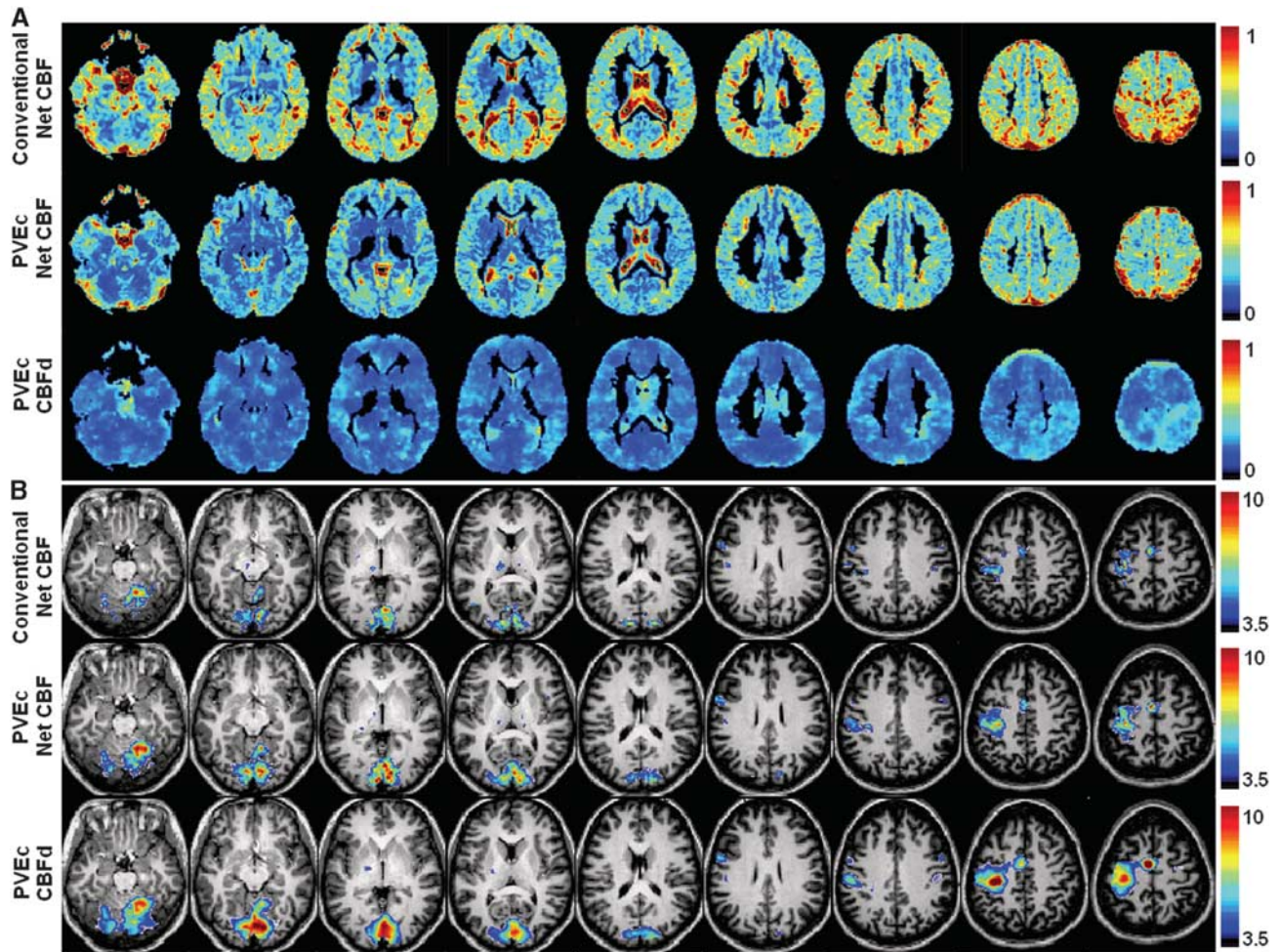


Figure 7 Comparison of signal-to-noise ratio of the partial volume effect corrected (PVEc) and conventional ASL methods. **(A)** Inter-subject coefficient of variation $(\sigma/\pi)_{\text{inter-subject}}$, for conventional net cerebral blood flow (CBF) (first row), PVEc net CBF (second row) and GM CBFd measurement (third row). Note that while the GM CBFd $(\sigma/\pi)_{\text{inter-subject}}$ is relatively uniform throughout, it varies substantially for the conventional net CBF, especially in regions with high tissue heterogeneity. **(B)** The effect of coefficient of variation on activation T-maps obtained with conventional net CBF (first row), PVEc net CBF (second row) and GM CBFd (third row) images.

spurious noise. Importantly, the test-retest reliability of the ASL signal in the primary motor cortex may be of particular interest in longitudinal studies of motor recovery after stroke (Feydy *et al*, 2002).

We showed that the CBFd, which is the CBF correlate obtained with the PVEc ASL method, is more sensitive in detecting functional changes in CBF than the net CBF, which is affected by the variability in voxel tissue heterogeneity across subjects, as well as the difference in voxel location across sessions of the same subject. Compared with the net CBF obtained with the conventional, PVE-uncorrected method, the SNR of the GM CBFd measure across the entire brain was ~ 2 times higher. This higher SNR of the PVEc method should lead to higher statistical power for experimental designs of ASL studies (Asllani *et al*, 2008b).

In addition to yielding a more accurate measurement of CBF than the conventional ASL method

(Asllani *et al*, 2008a), the PVEc CBFd measurement was found to have a lower inter- and intra-subject variance, thus increasing the sensitivity of detecting changes in CBF over time. In this study, we used healthy young volunteers. In studies involving populations with more considerable inter-subject differences in tissue content, and populations in which longitudinal changes in tissue content can occur (e.g., elderly and Alzheimer's disease patients), the CBFd images are expected to have an even more substantial impact on improving the sensitivity of ASL for detecting long term perfusion changes. Importantly, for studies of elderly populations, CBFd measure has the potential for detecting functional changes in the brain before structural differences occur.

To increase the accuracy of the CBF quantification, we combined the PVEc method with an acquisition protocol that was based on varying the length of the

labeling radiofrequency pulse to obtain ATT for GM at each voxel, independently. This novel approach yielded voxelwise ATT images that showed marked regional heterogeneity in ATT values even for voxels equidistant from the labeling plane. For example, the ATT for the cerebellum was about the same as for the more superior slices. The circle of Willis and the deep MCA and ACA regions had the shortest ATT (~200 to 300 ms), whereas the occipital lobe, the cerebellum, and the watershed territories had the longest (~800 to 1500 ms).

This study is the first to report on whole-brain regional differences in ATT, including the cerebellum. The ATT values obtained here are consistent with observations from a recent study by Hendrikse *et al* (2008), which is the only other study to explicitly reveal regional heterogeneity in ATT in a healthy young population. An earlier study by Wong *et al* (1997) also reported longer ATT in the occipital lobe, but lacked information on differences in ATT across other brain regions. Neither study corrected for the PVE in the ASL fractional signal change images used for the parametric fitting which, as our results show (Figure 2), can lead to a miss-estimation of ATT and, consequently, to a miss-estimation of CBF. In contrast, by using PVEc ASL, we were able to isolate the GM signal at each voxel and thus reduce the effect of WM and CSF, which have lower perfusion SNR and longer ATT values (Wong *et al*, 1997).

Another difference between this study and others that have sought to estimate ATT is that here we opted to vary the length of the labeling pulse rather than the length of the PLD; an approach similar to that adopted by Ye *et al* (1997). This was performed to lower the scanning time (as the PLD was kept at a minimum); *ceteris paribus*, the multiple-LD approach would be ~20% shorter. Perhaps more importantly, the multiple-LD approach should yield higher SNR as the inflection point in the curve is detected at an earlier time, before substantial attenuation of the signal has occurred. However, this statement is conjectural at this point as we did not directly compare the two methods.

One limitation of the ATT study presented herein is that the CASL pulse sequence used to acquire the multi-LD data did not include crusher gradients to separate the arterial and tissue signals. By isolating the arterial and tissue signal contributions, it should be possible to obtain a voxelwise template for tissue transit times, as well as to further improve the accuracy of the ATT estimation.

The ASL sequence used here has a short PLD, and was thus heavily weighted toward the vascular compartment (Figures 4 and 5). We opted for a relatively short PLD for two main reasons: First, because we sought to detect changes in CBF with task frequency ~30 times lower than previously published data (Wang *et al*, 2003), we wanted to boost the SNR (Detre and Alsop, 2000; Gonzalez-At

et al, 2000). However, to compensate for the low PLD, we applied a relatively long radiofrequency pulse (1.9 seconds) thus keeping the PLD+LD value comparable with other studies (Parkes *et al*, 2004; Rashid *et al*, 2004; Wang *et al*, 2004).

Second, because ATT are known to shorten during activation, using a short PLD would result in a larger ASL signal change between the baseline and activated states (Gonzalez-At *et al*, 2000). Gonzalez-At *et al* (2000) report a 250 and a 150 ms change in ATT because of activation in motor and visual cortex, respectively. However, the fitting of the data was performed on only 5 time points and no correction was done for the mixing of GM and WM signals. More research is needed to investigate regional dynamics of blood flow during activation and its effects on the estimation of both ATT and TTT.

The average baseline CBF_d values, as well as within-session Δ CBF_d, showed good reproducibility and were nearly identical for D1 and D30 sessions, in both the visual and motor cortex ROIs. On the subject level, however, there existed some variability in the measured perfusion across 1 month (Figure 6), which was more pronounced in the visual cortex. One possible explanation for this could be that, because the visual cortex is located lower in the brain, it is acquired with lower effective PLD and is thus more sensitive to any variation in the subject's ATT between the two imaging sessions. This explanation is consistent with the results from the PLD=1000 ms data, in which, although the difference in Δ CBF in the motor cortex between the PLD=500 ms and PLD=1000 ms acquisitions was negligible, in the visual cortex it was ~24 mL/100 g/min, corresponding to a 15% lower Δ CBF for PLD=1000 ms, relative to PLD=500 ms acquisition.

To date, fMRI has been most effective in mapping acute functional changes that typically occur over seconds and minutes, and has proven very useful in identifying brain regions that briefly respond to transient stimulation. However, many stimuli, even if their external source is transient, trigger a long-lasting neural response that is functionally meaningful. Furthermore, the pathophysiology of disease can be considered an internal stimulus, and most brain disorders cause brain dysfunction chronically not transiently. The technology introduced here is particularly well suited for mapping these long-term changes in normal and abnormal brain function.

Acknowledgements

The authors are grateful to Drs Truman R Brown, and Joy Hirsch for their crucial support, and Steven Dashnaw and Glenn Castillo for their assistance with data acquisition and transfer. The authors also thank the anonymous reviewers for their thorough and helpful critique of this work.

Disclosure/conflict of interest

The authors declare no conflict of interest.

References

- Aguirre GK, Detre JA, Zarahn E, Alsop DC (2002) Experimental design and the relative sensitivity of BOLD and perfusion fMRI. *Neuroimage* 15:488–500
- Alsop DC, Detre JA (1996) Reduced transit-time sensitivity in noninvasive magnetic resonance imaging of human cerebral blood flow. *J Cereb Blood Flow Metab* 16:1236–49
- Alsop DC, Detre JA (1998) Multisection cerebral blood flow MR imaging with continuous arterial spin labeling. *Radiology* 208:410–6
- Ashburner J, Friston KJ (2005) Unified segmentation. *Neuroimage* 26:839–51
- Asllani I, Borogovac A, Brown TR (2008a) Regression algorithm correcting for partial volume effects in arterial spin labeling MRI. *Magn Reson Med* 60:1362–71
- Asllani I, Borogovac A, Wright C, Sacco R, Brown TR, Zarahn E (2008b) An investigation of statistical power for continuous arterial spin labeling imaging at 1.5 T. *Neuroimage* 39:1246–56
- Asllani I, Borogovac A, Brown TR, Hirsch J, Krakauer JW (2009a) Limit of detection of localized absolute changes in CBF using arterial spin labeling (ASL) MRI. In: Proceedings of the 17th Annual Meeting of International Society of Magnetic Resonance in Medicine (ISMRM). Honolulu, Hawaii
- Asllani I, Habeck C, Borogovac A, Brown TR, Brickman AM, Stern Y (2009b) Separating function from structure in perfusion imaging of the aging brain. *Hum Brain Map* 30:2927–35
- Bandettini PA (2001) Selection of the optimal pulse sequence for functional MRI. In: *Functional MRI: An Introduction to Methods* (Jezzard P, Matthews PM, Smith SM, eds) Oxford University Press: New York, NY
- Detre JA, Alsop DC (2000) Perfusion fMRI with arterial spin labeling. In: *Functional MRI* (Moonen CT, Bandettini PA, eds) Heidelberg: Springer, 47–62
- Ethofer T, Mader I, Seeger U, Helms G, Erb M, Grodd W, Ludolph A, Klose U (2003) Comparison of longitudinal metabolite relaxation times in different regions of the human brain at 1.5 and 3 Tesla. *Magn Reson Med* 50:1296–301
- Feydy A, Carlier R, Roby-Brami A, Bussel B, Cazalis F, Pierot L, Burnod Y, Maier MA (2002) Longitudinal study of motor recovery after stroke: recruitment and focusing of brain activation. *Stroke* 33:1610–7
- Friston KJ, Williams S, Howard R, Frackowiak RS, Turner R (1996) Movement-related effects in fMRI time-series. *Magn Reson Med* 35:346–55
- Gelman N, Gorell JM, Barker PB, Savage RM, Spickler EM, Windham JP, Knight RA (1999) MR imaging of human brain at 3.0 T: preliminary report on transverse relaxation rates and relation to estimated iron content. *Radiology* 210:759–67
- Golay X, Hendrikse J, Lim TC (2004) Perfusion imaging using arterial spin labeling. *Top Magn Reson Imaging* 15:10–27
- Gonzalez-At JB, Alsop DC, Detre JA (2000) Cerebral perfusion and arterial transit time changes during task activation determined with continuous arterial spin labeling. *Magn Reson Med* 43:739–46
- Greenman RL, Shirosky JE, Mulkern RV, Rofsky NM (2003) Double inversion black-blood fast spin-echo imaging of the human heart: a comparison between 1.5T and 3.0T. *J Magn Reson Imaging* 17:648–55
- Hendrikse J, Petersen ET, van Laar PJ, Golay X (2008) Cerebral border zones between distal end branches of intracranial arteries: MR imaging. *Radiology* 246:572–80
- Hermes M, Hagemann D, Britz P, Lieser S, Rock J, Naumann E, Walter C (2007) Reproducibility of continuous arterial spin labeling perfusion MRI after 7 weeks. *MAGMA* 20:103–15
- Herscovitch P, Raichle ME (1985) What is the correct value for the brain–blood partition coefficient for water? *J Cereb Blood Flow Metab* 5:65–9
- Hirohiko K, Kabasawa H, Yonekura Y, Itak H (2004) Cerebral perfusion measurements using continuous arterial spin labeling: accuracy and limits of a quantitative approach. *Inter Congress Series* 1265:238–47
- Kimura H, Kabasawa H, Yonekura Y, Itoh H (2004) Cerebral perfusion measurements using continuous arterial spin labeling: accuracy and limits of a quantitative approach. *Inter Congress Series* 1265:238–47
- Maldjian JA, Laurienti PJ, Kraft RA, Burdette JH (2003) An automated method for neuroanatomic and cytoarchitectonic atlas-based interrogation of fMRI data sets. *Neuroimage* 19:1233–9
- Maldjian JA, Laurienti PJ, Burdette JH (2004) Precentral gyrus discrepancy in electronic versions of the Talairach atlas. *Neuroimage* 21:450–5
- Ogawa S, Menon RS, Tank DW, Kim SG, Merkle H, Ellermann JM, Ugurbil K (1993) Functional brain mapping by blood oxygenation level-dependent contrast magnetic resonance imaging. A comparison of signal characteristics with a biophysical model. *Biophys J* 64:803–12
- Parkes LM, Tofts PS (2002) Improved accuracy of human cerebral blood perfusion measurements using arterial spin labeling: accounting for capillary water permeability. *Magn Reson Med* 48:27–41
- Parkes LM, Rashid W, Chard DT, Tofts PS (2004) Normal cerebral perfusion measurements using arterial spin labeling: reproducibility, stability, and age and gender effects. *Magn Reson Med* 51:736–43
- Pereira AC, Huddleston DE, Brickman AM, Sosunov AA, Hen R, McKhann GM, Sloan R, Gage FH, Brown TR, Small SA (2007) An *in vivo* correlate of exercise-induced neurogenesis in the adult dentate gyrus. *Proc Natl Acad Sci USA* 104:5638–43
- Rashid W, Parkes LM, Ingle GT, Chard DT, Toosy AT, Altmann DR, Symms MR, Tofts PS, Thompson AJ, Miller DH (2004) Abnormalities of cerebral perfusion in multiple sclerosis. *J Neurol Neurosurg Psychiatry* 75:1288–93
- Stanisz GJ, Odobina EE, Pun J, Escaravage M, Graham SJ, Bronskill MJ, Henkelman RM (2005) T1, T2 relaxation and magnetization transfer in tissue at 3T. *Magn Reson Med* 54:507–12
- Wang J, Alsop DC, Li L, Listerud J, Gonzalez-At JB, Schnell MD, Detre JA (2002) Comparison of quantitative perfusion imaging using arterial spin labeling at 1.5 and 4.0 Tesla. *Magn Reson Med* 48:242–54
- Wang J, Aguirre GK, Kimberg DY, Roc AC, Li L, Detre JA (2003) Arterial spin labeling perfusion fMRI with very low task frequency. *Magn Reson Med* 49:796–802
- Wang J, Li L, Roc AC, Alsop DC, Tang K, Butler NS, Schnell MD, Detre JA (2004) Reduced susceptibility effects in perfusion fMRI with single-shot spin-echo EPI acquisitions at 1.5 Tesla. *Magn Reson Imaging* 22:1–7

- Wang J, Zhang Y, Wolf RL, Roc AC, Alsop DC, Detre JA (2005) Amplitude-modulated continuous arterial spin-labeling 3.0-T perfusion MR imaging with a single coil: feasibility study. *Radiology* 235:218–28
- Wansapura JP, Holland SK, Dunn RS, Ball Jr WS (1999) NMR relaxation times in the human brain at 3.0 tesla. *J Magn Reson Imaging* 9:531–8
- Williams DS, Detre JA, Leigh JS, Koretsky AP (1992) Magnetic resonance imaging of perfusion using spin inversion of arterial water. *Proc Natl Acad Sci USA* 89:212–6
- Wong EC, Buxton RB, Frank LR (1997) Implementation of quantitative perfusion imaging techniques for functional brain mapping using pulsed arterial spin labeling. *NMR Biomed* 10:237–49
- Ye FQ, Mattay VS, Jezzard P, Frank JA, Weinberger DR, McLaughlin AC (1997) Correction for vascular artifacts in cerebral blood flow values measured by using arterial spin tagging techniques. *Magn Reson Med* 37:226–35
- Zarahn E, Aguirre G, D'Esposito M (1997) A trial-based experimental design for fMRI. *Neuroimage* 6:122–38